Cyclophanes

International Edition: DOI: 10.1002/anie.201605286
German Edition: DOI: 10.1002/ange.201605286

Homochiral [2.2]Paracyclophane Self-Assembly Promoted by Transannular Hydrogen Bonding

*Danielle E. Fagnani, Michael J. Meese, Jr., Khalil A. Abboud, and Ronald K. Castellano**

Abstract: *[2.2]paracyclophane (pCp), unlike many π-building blocks, has been virtually unexplored in supramolecular constructs. Reported here is the synthesis and characterization of the first pCp derivatives capable of programmed self-assembly into extended cofacial π-stacks in solution and the solid state. The design employs transannular (intramolecular) hydrogen bonds (H-bonds), hitherto unstudied in pCps, between pseudo-ortho-positioned amides of a pCp-4,7,12,15-tetracarboxamide (pCpTA) to preorganize the molecules for intermolecular H-bonding with π-stacked neighbors. X-ray crystallography confirms the formation of homochiral, one-dimensional pCpTA stacks helically laced with two H-bond strands. The chiral sense is dictated by the planar chirality (R_p or S_p) of the pCpTA monomers. A combination of NMR, IR, and UV/Vis studies confirms the formation of the first supramolecular pCp polymers in solution.*

[2.2]Paracyclophane (pCp; Figure 1a) has enticed academic and commercial curiosity for over half a century.[1] The rigid connectivity and positioning of its "bent and battered benzene rings"[2] are the basis for through-space (transannular π–π) and through-bond [σ(bridge)–π(deck)] interactions[3] which strongly perturb the chemical, optical, and electronic properties of the molecule. The synthetic chemistry of pCp is quite mature and allows functional groups to be precisely positioned on the rings and bridges[2,4]—two common ring substitution patterns are shown in Figure 1b. Synthetic organic chemists continue to use the planar chirality associated with appropriately functionalized pCps in ligand and catalyst design to great effect,[5] while work by the groups of Bazan,[6] Chujo,[7] Collard,[8] and others[9] has beautifully evaluated the consequences of through-space conjugation on the properties of covalent π-conjugated oligomers and polymers featuring embedded pCps. Indeed, the pCp building block remains attractive for organic optoelectronic applications ranging from nonlinear optics[10] to photovoltaics.[11]

The prospect of delocalized electronic states emerging for extended π-stacked cyclophanes dates back to the seminal work of the groups of Chow,[12] Misumi,[13] and Staab,[14] whose tediously prepared multitiered structures (e.g., Figure 1c) showed, for example, longer wavelength absorption and emission maxima upon increasing the number of intervening benzene rings. The single-molecule conductance of such constructs has only recently been measured.[15] Covalent systems which enforce much looser interactions between pCp rings[7a–c,8b,c,9c] nonetheless show evidence for delocalized "phane" states through π-stacking. It therefore comes as a surprise that unlike many π-conjugated molecules for which robust self-assembly recipes have been established[16] to encourage their predictable and even chiral one-dimensional (1D) supramolecular ordering in solution and the solid state, pCps have hardly been studied in this regard.[17]

Reported here is the first self-assembly strategy to promote the stacking of [2.2]paracyclophanes to produce 1D supramolecular architectures. The design relies on judiciously installed transannular hydrogen-bonding (H-bonding) interactions—hitherto unstudied in this class of molecules—which predispose the chiral monomers for stereospecific, noncovalent polymerization. Assembly formation has been confirmed in the solid state through single-crystal X-ray analysis, and in solution by NMR, UV/Vis, and IR spectroscopy. Despite only two hydrogen bonds connecting adjacent pCps, the association strength in nonpolar organic solvents (e.g., cyclohexane) is sufficiently high for viscous solutions to result at millimolar concentrations. The overall design should be adaptable to a variety of cyclophane frameworks and promote their exploration in new functional contexts.

Our pCp self-assembly design borrows conceptually from benzene-1,3,5-tricarboxamides (BTAs), molecules which reliably form 1D assemblies through threefold H-bonding between the tilted amides of adjacent π-stacked monomers (Figure 1d). The BTA assembly paradigm has found numerous applications across the materials and biomedical sciences,[18] and is sufficiently robust for classroom experiments.[19] One approach to porting the motif to [2.2]paracyclophane employs pCp-4,7,12,15-tetracarboxamide (pCpTA). The substitution pattern together with the pCp bridged structure demand formation of intramolecular N–H···O=C hydrogen bonds between pseudo-*ortho*-disposed amides. Reminiscent of the work of Nuckolls and co-workers with persubstituted (crowded) BTAs,[20] the pCp monomer becomes preorganized for intermolecular H-bonding with two π-stacked neighbors. Gas-phase calculations (DFT M06-2X/6-31 + G*)[21] of a representative monomer (Figure 1e), where $R = CH_3$, identify two C_2-symmetric low-energy conformations, *anti* and *syn*, which differ with respect to their H-bonding (i.e., amide carbonyl) directionality and energy (the former is more stable by 0.2 kcal mol^{-1}). The amide torsion angles (defined by the C=O and pCp aryl planes), ϕ_1–ϕ_4, are similar between the isomers ($\phi_1 \approx \phi_3 \approx 35°$; $\phi_2 \approx \phi_4 \approx -154°$) and support good linearity and optimized distances (N···C=O ≈ 2.9 Å) between

[*] D. E. Fagnani, M. J. Meese Jr., Dr. K. A. Abboud, Prof. Dr. R. K. Castellano
Department of Chemistry, University of Florida
P.O. Box 117200, Gainesville, FL 32611 (USA)
E-mail: castellano@chem.ufl.edu

Supporting information and the ORCID identification number(s) for the author(s) of this article can be found under http://dx.doi.org/10.1002/anie.201605286.

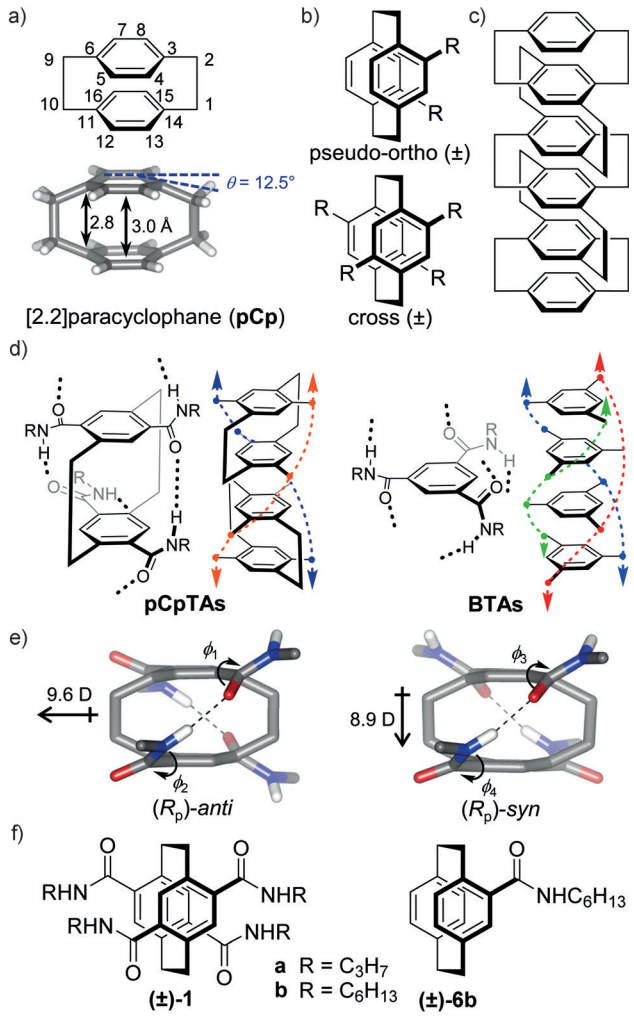

Figure 1. π-Stacked [2.2]paracyclophanes (pCps). a) Top, structure of [2.2]paracyclophane (pCp) and its standard carbon numbering. Bottom, X-ray crystal structure (data at 15 K) of pCp with transannular distances and benzene ring deformation indicated.[33] b) Familiar names of two pCp substitution patterns; planar chirality is indicated (±). c) A sixfold layered cyclophane. See Ref. [13b]. d) The design of pCps capable of self-assembly through hydrogen bonding: Intramolecular (transannular) hydrogen bonds (dotted black lines) in a pCp-4,7,12,15-tetracarboxamide (pCpTA) predispose the molecule for self-complementary association with a stacked neighbor. The design draws inspiration from the benzene-1,3,5-tricarboxamide (BTA) assembly motif. Monomer configuration (i.e., R_p for pCpTA) and conformation (i.e., *anti* for pCpTA) are representative. Dashed colored lines depict the double and triple helical hydrogen-bond lacing for the pCpTAs and BTAs, respectively. e) Gas-phase, geometry-minimized structures (M06-2X/6-31 + G*) of (R_p)-*anti* and (R_p)-*syn* pCpTA monomers where R = CH_3. Some hydrogen atoms have been removed for clarity. Geometric parameters: N···C=O = 2.93 Å; $\phi_1 = 35.8°$; $\phi_2 = -152°$; $\phi_3 = 33.9°$; $\phi_4 = -155°$. Calculated molecular dipole moments are shown in Debye units (D). f) Compounds prepared and studied in this work.

the H-bond donors and acceptors. Computational comparison of the pCpTA conformations to those of pCp-4-monocarboxamide, pCp-4,12-dicarboxamide, and pCp-4,16-dicarboxamide models (see Figure S2 in the Supporting Information) further shows that the estimated intramolecular H-bond energy (ca. 8 kcal mol^{-1}) more than compensates for a slightly unfavorable amide positioning in the H-bonded arrangement (which costs ca. 1 kcal mol^{-1}).

Upon pCpTA monomer self-assembly, as shown schematically (Figure 1 d), two (as opposed to three for the BTAs) strands of H-bonds will helically "lace up" a 1D supramolecular structure, evocative of both polypeptides and duplex DNA. Unlike the BTA system, for which the monomer is inherently achiral and assembly stereocontrol can only be achieved through remote chiral induction (e.g., the introduction of chiral side chains), the helical sense of pCpTA assembly is dictated by the planar chirality of the monomers (R_p or S_p). One consequence is that pCpTA linear assembly is homochiral,[22] that is, each member of a propagating 1D stack must share the same absolute stereochemistry. The system joins just a handful of others whereby chiral self-sorting in supramolecular polymerization is realized in the absence of chiral carbon centers.[23] A final distinction between the pCpTAs and BTAs worth noting is related to their assembly polarity. While the latter boasts a permanent assembly macrodipole (which amplifies upon assembly growth) regardless of amide directionality, only the *syn* conformation of pCpTA (with its amides pointed in the stacking direction) is expected to behave similarly. The *anti* conformation, while polar as a monomer, should lead to effectively nonpolar nanorods upon 1D noncovalent polymerization. It is interesting to consider if the reduction in dipole which accompanies assembly can drive pCpTA self-association in a nonpolar solvent.

The synthesis of (±)-**1** (Figure 1 f; see Scheme S1) progressing through intermediates **2**–**5** began from commercially available pCp, which was tetrabrominated in the manner reported by Reich and Cram,[24] converted into its tetraacid through lithium–halogen exchange followed by quenching with CO_2, as reported by Rozenberg and co-workers for the synthesis of pCp mono- and diacids,[25] and finally converted into the aliphatic amide derivatives (±)-**1a** and (±)-**1b** using standard chemistry. The hexyl version affords particularly good solubility in organic solvents. A similar synthetic approach was used to prepare monoamide (±)-**6b**, which is useful as a comparator molecule to report on the hydrogen-bonding properties of (±)-**1**.

Slow evaporation of an ethanol solution of (±)-**1a** produced needle-like crystals of sufficient quality for single-crystal X-ray diffraction. The data (Figure 2), after extensive refinement (due to primarily side-chain disorder), unambiguously confirms the intended pCpTA assembly design. Three configurationally equivalent [i.e., (R_p)-**1a**$_{anti}$ or (S_p)-**1a**$_{anti}$] but crystallographically independent pCpTA molecules constitute the asymmetric unit. The trimer stacks derived from (S_p)-**1a**$_{anti}$ and (R_p)-**1a**$_{anti}$ are shown in Figure 2 a. Revealed experimentally is an average intramolecular (transannular) H-bond (N···C=O) distance of 2.81 Å, nearly identical to the average intermolecular H-bond distance of 2.77 Å. Accompanying the well-optimized H-bonding distances are average amide torsion angles ($\phi_1 \approx -38°$; $\phi_2 \approx -141°$) which are reasonably consistent with those predicted from DFT calculations. While the average intramolecular distance between

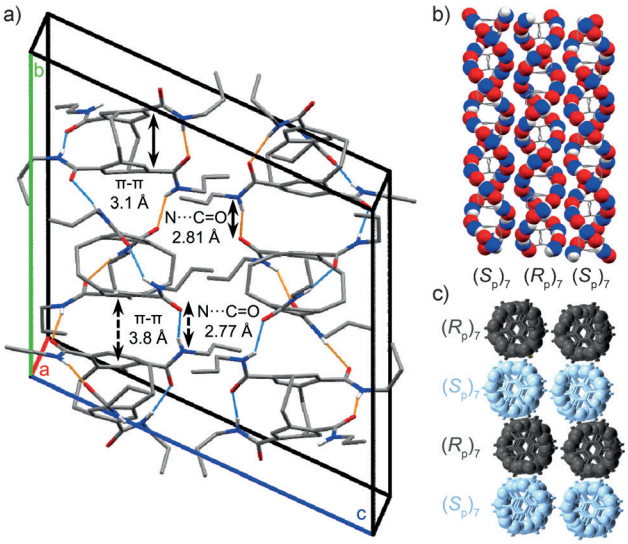

Figure 2. X-ray crystal structure of pCp-4,7,12,15-tetracarboxamide (±)-**1a**.[34] a) Unit cell containing each enantiomorphic asymmetric unit. The two helical H-bond laces are denoted with differently colored dashed lines. Centroid-to-centroid benzene distances and H-bonding distances are shown. b) pCp packing. Side view of extended pCp stacks. c) Packing diagram showing multiple (S_p)-**1a**$_{anti}$ (light blue) and (R_p)-**1a**$_{anti}$ (dark gray) stacks from a top-down view. Atom color code: blue N, gray C, red O, and white H. In b,c) atoms participating in H-bonding are shown as spheres for clarity. Alkyl chains and disorder have also been omitted for clarity.

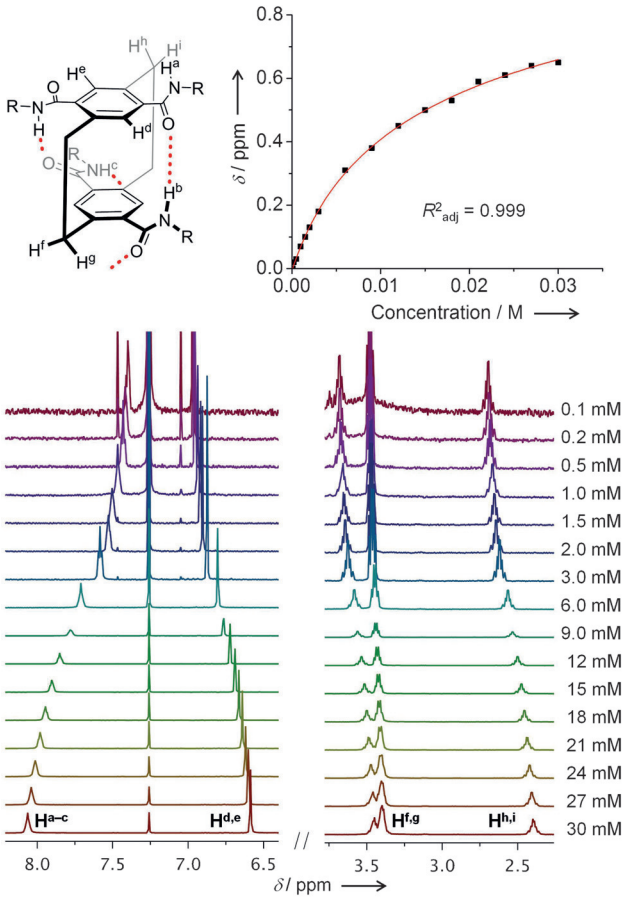

Figure 3. Solution-phase self-assembly of (±)-**1b** reported by variable-concentration ^{1}H NMR spectroscopy (0.1–30×10^{-3} M in $CDCl_3$ at 25 °C). Top left: molecular structure of (±)-**1b** with protons labeled. Top right: nonlinear curve fitting of concentration-dependent NH chemical shift data ($CDCl_3$) fit to an isodesmic model.

aryl ring centroids (3.1 Å) is fixed and consequently short, the intermolecular centroid-to-centroid distances are on-average larger, 3.8 Å (the closest intermolecular $C_{aryl}\cdots C_{aryl}$ distance is 3.4 Å). The increased distance reflects some monomer-to-monomer wobbling along the 1D chain, presumably a result of the molecules' negotiating favorable H-bonding interactions and unfavorable repulsions between the distorted aromatic ring surfaces. As testament to the latter, a search of the Cambridge Crystallographic Database reveals just eight structures (out of ca. 500 possibilities) with close (≤ 4.0 Å) and mostly slip-stacked intermolecular pCp π-surfaces (see Figure S10). Even so, dynamic solution environments likely support transiently close (and more typical) π-stacking distances for assembled pCpTAs.

While the *anti* conformation of the pCpTA monomer is perhaps slightly favored, its selection in the crystal is probably governed by longer range interactions which also dictate the columnar packing arrangement. The helical sense of the antiparallel H-bonding laces between the homochiral stacks, [(R_p)-**1a**$_{anti}$]$_n$ or [(S_p)-**1a**$_{anti}$]$_n$, are naturally opposite as dictated by monomer planar chirality. The [(R_p)-**1a**$_{anti}$]$_n$ and [(S_p)-**1a**$_{anti}$]$_n$ stacks closely pack as shown in Figure 2c (the alkyl side chains have been removed for clarity). Interesting to note is that while the interface between the individual columns is filled with alkyl side chains, the interface associated with the shortest intercolumnar distance (10 vs. 12 Å) involves amides pointing in the same and not opposite directions.

^{1}H NMR data acquired for soluble (±)-**1b** in $CDCl_3$ from 0.1–30 mM (Figure 3) shows concentration-dependent chemical shift changes consistent with the self-assembly shown by X-ray crystallography. Specifically, upon increasing the concentration, the amide NH resonance [which, assuming the *anti* conformation, represents the weighted average of three NH environments: solvent exposed (H^a), intramolecularly H-bonded (H^b), and intermolecularly H-bonded (H^c)] shifts downfield (to ca. 8.1 ppm; Δδ ca. 0.6 ppm), and the time-averaged aromatic pCp protons (H^d and H^e) shift upfield (to ca. δ = 6.6 ppm; Δδ ca. 0.3 ppm). Smaller, but equally informative upfield shifts are observed for the diastereotopic methylene protons (H^{f-i}) on the bridges. Given that significant monomer conformational changes are not expected upon assembly, the upfield C–H shifts presumably arise from the ring current effect induced by π-stacking. The downfield shift of the amide proton is diagnostic of H-bonded assembly, and nonlinear curve fitting of the concentration-dependent data to an isodesmic (equal-K)[26] self-assembly model provides K_{el} = 63 ± 5 M^{-1} (similar values are obtained from the other protons; see the Supporting Information). The results contrast with those of (±)-**6b**, which shows an upfield (δ = 5.5 ppm in $CDCl_3$) and concentration invariant (from 0.1–30 mM) amide NH resonance.

Further evidence for self-association by H-bonding comes through complementary FT-IR analysis (Figure 4a and Fig-

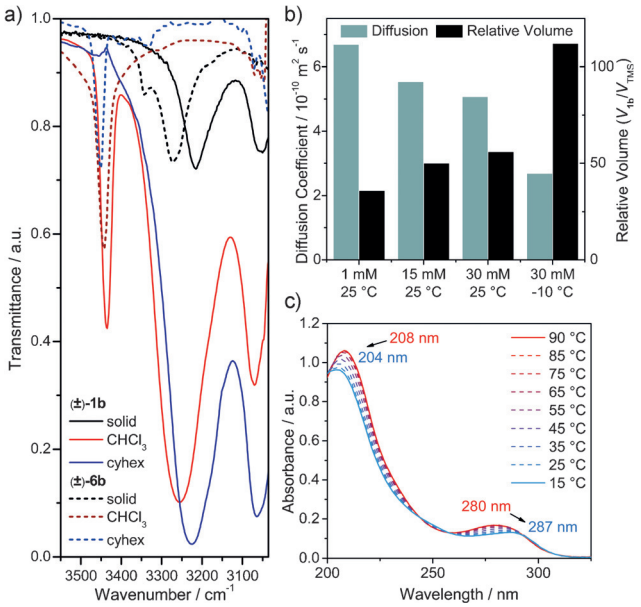

Figure 4. Solution-phase self-assembly of (±)-**1b** versus non-assembling pCp-4-monocarboxamide comparator (±)-**6b**. [a] IR spectrum of the N–H stretch region (3550–3050 cm^{-1}) of (±)-**1b** (solid lines) and (±)-**6b** (dashed lines) in the solid state (black lines), at 30×10^{-3} M in chloroform (red lines), and at 30×10^{-3} M in cyclohexane (abbreviated cyhex; blue lines). N–H stretch energies are provided in the text. [b] Graphical representation of DOSY data obtained for (±)-**1b** at variable concentrations and temperatures in $CDCl_3$, thus indicating a decrease in the diffusion coefficient and increase of hydrodynamic radius relative to a TMS standard upon aggregation. c) Temperature-dependent absorption spectra (corrected for temperature-dependent solvent density changes) of (±)-**1b** (40×10^{-6} M in MCH) collected with a constant cooling rate of 1 °C per minute. Arrows indicate the direction of decreasing temperature.

ures S11–S15). In the solid state, a predominant and broad N–H stretch is observed for (±)-**6b** at 3276 cm^{-1} (associated with intermolecular H-bonding), while two broad N–H stretches [ascribable to weaker, intermolecular (3215 cm^{-1}) and stronger, intramolecular (3052 cm^{-1}) H-bonding] are found for (±)-**1b**. At 30 mM in $CHCl_3$, (±)-**6b** shows only a sharp, solvent-exposed N–H stretch (3442 cm^{-1}), a resonance also found for (±)-**1b** (3437 cm^{-1}). Two additional broad N–H stretches are observed for (±)-**1b** (3257 and 3068 cm^{-1}), thus mirroring the solid-state behavior and consistent with H-bond association at these concentrations.

The equilibrium constant for (±)-**1b** is relatively small in chloroform, but reasonable given the number of intermonomer H-bonding interactions, and a bit larger than some BTAs[27] ($K=15\pm5\,M^{-1}$). Indeed, DOSY NMR measurements in $CDCl_3$ (Figure 4b) could be used to verify supramolecular growth through translational diffusion coefficients (D) obtained at various concentrations and temperatures. For (±)-**1b** at 25 °C, D (10^{-10} m^{2}s^{-1}) decreases from 6.7 ± 0.1 at 1 mM, to 5.5 ± 0.1 at 15 mM, to 5.1 ± 0.1 at 30 mM. The latter value expectedly decreases further (to 2.7 ± 0.1) upon lowering the temperature to −10 °C. The trends, consistent with pCp self-assembly, are alternatively expressed through estimated hydrodynamic volumes relative to a non-aggregating internal reference tetramethylsilane (TMS).[28] The changes observed in relative volume, V_{1b}/V_{TMS}, upon variation of concentration and temperature [36 ± 2 (1 mM, 25 °C), 50 ± 2 (15 mM, 25 °C), 56 ± 2 (30 mM, 25 °C), 112 ± 9 (30 mM, −10 °C)], are consistent with pCp self-association and the trends discussed above.

A dramatic change in solution behavior is observed when (±)-**1b** is dissolved in a less-polar hydrocarbon solvent (e.g., cyclohexane or methylcyclohexane). Even at mM concentrations, the solutions are considerably viscous (see the movie in the Supporting Information), a hallmark macroscopic property of H-bonded supramolecular polymers[29], thus suggesting a significant boost in association strength. While this is expected from the standpoint of H-bonding, it must also mean that the pCp π-stacking is, at the very least, accommodated under these conditions. The solution spectroscopic data is consistent with the macroscopic result. ^{1}H NMR analysis in [D_{12}]cyclohexane, for example, shows concentration invariant chemical shifts for (±)-**1b** between 0.1–1.0 mM. The result confirms a persistent aggregated state at even this level of dilution, further evidenced by slow monomer exchange on the NMR timescale which affords two broad and downfield ($\delta_{Hb}=9.6$ ppm; $\delta_{Hc}=8.8$ ppm) NH resonances. Meanwhile, the amide NH resonance of (±)-**6b** remains upfield ($\delta=5.2$ ppm, 30 mM in [D_{12}]cyclohexane; see Figures S24 and S25). FT-IR data in cyclohexane is fully consistent with the ^{1}H NMR data, thus showing exclusively two H-bonded N–H stretches for (±)-**1b** and one solvent-exposed N–H stretch for (±)-**6b** (Figure 4a). Worth noting, while the N–H stretch of (±)-**1b** associated with intramolecular H-bonding (3063 cm^{-1}) in cyclohexane is comparable to chloroform (3068 cm^{-1}), the intermolecularly H-bonded NH shows a stretch at lower energy (3222 cm^{-1}) consistent with stronger H-bonding in this solvent.

Finally, the larger K_{el} value ($>10^4\,M^{-1}$, estimated from the ^{1}H NMR dilution data) provides the opportunity to evaluate assembly by UV/Vis spectroscopy, which can report on both inter- and intramolecular pCp electronic interactions. Quite preliminary frontier MO analysis of [(R_p)-**1a**$_{anti}$]$_2$ in the gas phase (DFT M06-2X/6-31+G*) shows that through-space (intermonomer) orbital delocalization could accompany dimerization (see Figure S6). Absorption spectra of (±)-**1b** (40 μM) recorded at various temperatures (15–90 °C) in methylcyclohexane (MCH) show a hypsochromic shift of the higher energy ($\lambda_{max}=208$ nm at 90 °C; 204 nm at 15 °C) transition and bathochromic shift of the lower energy ($\lambda_{max}=280$ nm at 90 °C; 287 nm at 15 °C) transition, with clean isosbestic points, upon cooling (aggregation; Figure 4c). The former absorption presumably originates from a π–π* transition involving H-aggregated benzene decks,[30] while the latter cyclophane band reports on the distance between and the deformation of the pCp benzene rings,[31] deformation which occurs upon assembly. A bathochromic shift and attenuated intensity of the cyclophane band has been reported as paracyclophane decks are positioned closer in space.[32] A similar trend of the cyclophane band is observed for (±)-**1b** (40 μM) when comparing chloroform ($\lambda_{max}=283$ nm) and methylcyclohexane ($\lambda_{max}=287$ nm) spectra, where the latter solvent is able to support stronger hydrogen

bonds (see Figure S27). As further evidence that the temperature-dependent absorption energy changes are induced by self-assembly, no hypso- or bathochromic shifts are observed for either (±)-**6b** in methylcyclohexane (see Figure S30) or for (±)-**1b** in ethanol (see Figure S31), a solvent which effectively competes for hydrogen bonds. The temperature-dependent spectral changes of the high-energy band, which report on the degree of polymerization, do not cleanly fit an equal-*K* model (see Figure S32),[26b] thus suggesting a more complex relationship between the absorption changes and assembly mechanism. The high-energy band and cyclophane band for (±)-**1b** maintain the same absorption maxima ($\lambda =$ 207 nm and 287 nm, respectively) and obey Beer's law (see Figures S28 and S29) in methylcyclohexane across a broad concentration range (2.5–120 μM). Taken together with the ^{1}H NMR dilution data for (±)-**1b** in [D_{12}]cyclohexane, this data indicates that the concentration range remains above what is required to observe concentration-dependent aggregation behavior. In other words the solvated species remain in largely aggregated form within this range at 25 °C. Forthcoming studies will probe the assembly characteristics more deeply through additional spectroscopic measurements.

We have introduced the first pCps, specifically pCp-4,7,12,15-tetracarboxamides (pCpTAs), capable of spontaneous organization into well-defined supramolecular assemblies. The 1D arrangements are homochiral, with each column comprising monomers sharing the same planar-chiral configuration, and helically laced-up by two strands of anti-parallel hydrogen bonds. A single-crystal X-ray structure has confirmed the supramolecular arrangement in the solid state and NMR, IR, and UV/Vis spectroscopic measurements have shown its persistence in solution. The molecular design is the first to feature cooperative transannular (intramolecular) and intermolecular H-bonds along a propagating stack of aromatic molecules. Early indications are that this new assembly paradigm is robust and should accommodate monomer-level structural tailoring for specific applications in materials science and organic optoelectronics. Spectroscopic studies are underway to elucidate supramolecular polymerization mechanism details and explore possible long-range, through-space charge/energy transport. Results along these lines will be reported in due course.

Acknowledgments

Preliminary experiments were funded by the University of Florida and the National Science Foundation CAREER program (CHE-0548003). We are grateful to the University of Florida and the National Science Foundation (CHE-0821346) for funding the X-ray equipment. We also thank Ashley Felts for her assistance with the X-ray crystallographic analysis, Dr. Ion Ghiviriga for assistance with the DOSY data collection, and Jonathan Grolms for technical assistance with the synthesis of (±)-**6b**. D.E.F. acknowledges a fellowship from the UF Nanoscience Institute for Medical & Engineering Technology.

Keywords: chirality · cyclophanes · hydrogen bonding · self-assembly · supramolecular chemistry

How to cite: *Angew. Chem. Int. Ed.* **2016**, *55*, 10726–10731
Angew. Chem. **2016**, *128*, 10884–10889

[1] a) C. J. Brown, A. C. Farthing, *Nature* **1949**, *164*, 915–916; b) D. J. Cram, H. Steinberg, *J. Am. Chem. Soc.* **1951**, *73*, 5691–5704.
[2] D. J. Cram, J. M. Cram, *Acc. Chem. Res.* **1971**, *4*, 204–213.
[3] a) E. Heilbronner, Z.-z. Yang in *Cyclophanes II*, *Vol. 115* (Ed.: F. Vögtle), Springer, Berlin, **1983**, pp. 1–55; b) H. Dodziuk, V. Vetokhina, H. Hopf, R. Luboradzki, P. Gaweł, J. Waluk, *J. Chem. Phys.* **2012**, *136*, 074201.
[4] *Modern Cyclophane Chemistry* (Eds.: R. Gleiter, H. Hopf), Wiley-VCH, Weinheim, **2005**.
[5] J. Paradies, *Synthesis* **2011**, 3749–3766.
[6] G. C. Bazan, *J. Org. Chem.* **2007**, *72*, 8615–8635.
[7] a) Y. Morisaki, Y. Chujo, *Tetrahedron Lett.* **2005**, *46*, 2533–2537; b) Y. Morisaki, T. Murakami, Y. Chujo, *Macromolecules* **2008**, *41*, 5960–5963; c) Y. Morisaki, T. Murakami, T. Sawamura, Y. Chujo, *Macromolecules* **2009**, *42*, 3656–3660; d) Y. Morisaki, Y. Chujo, *Polym. Chem.* **2011**, *2*, 1249–1257.
[8] a) F. Salhi, D. M. Collard, *Adv. Mater.* **2003**, *15*, 81–85; b) S. P. Jagtap, D. M. Collard, *J. Am. Chem. Soc.* **2010**, *132*, 12208–12209; c) S. P. Jagtap, S. Mukhopadhyay, V. Coropceanu, G. L. Brizius, J.-L. Brédas, D. M. Collard, *J. Am. Chem. Soc.* **2012**, *134*, 7176–7185.
[9] a) B. König, B. Knieriem, A. D. Meijere, *Chem. Ber.* **1993**, *126*, 1643–1650; b) L. Guyard, M. Nguyen Dinh An, P. Audebert, *Adv. Mater.* **2001**, *13*, 133–136; c) D. Bléger, D. Kreher, F. Mathevet, A.-J. Attias, I. Arfaoui, G. Metgé, L. Douillard, C. Fiorini-Debuisschert, F. Charra, *Angew. Chem. Int. Ed.* **2008**, *47*, 8412–8415; *Angew. Chem.* **2008**, *120*, 8540–8543.
[10] G. P. Bartholomew, M. Rumi, S. J. K. Pond, J. W. Perry, S. Tretiak, G. C. Bazan, *J. Am. Chem. Soc.* **2004**, *126*, 11529–11542.
[11] Y. Yang, G. Zhang, C. Yu, C. He, J. Wang, X. Chen, J. Yao, Z. Liu, D. Zhang, *Chem. Commun.* **2014**, *50*, 9939–9942.
[12] D. T. Longone, H. S. Chow, *J. Am. Chem. Soc.* **1970**, *92*, 994–998.
[13] a) T. Otsubo, S. Mizogami, I. Otsubo, Z. Tozuka, A. Sakagami, Y. Sakata, S. Misumi, *Bull. Chem. Soc. Jpn.* **1973**, *46*, 3519–3530; b) T. Otsubo, Z. Tozuka, S. Mizogami, Y. Sakata, S. Misumi, *Tetrahedron Lett.* **1972**, *13*, 2927–2930.
[14] H. A. Staab, U. Zapf, A. Gurke, *Angew. Chem. Int. Ed. Engl.* **1977**, *16*, 801–803; *Angew. Chem.* **1977**, *89*, 841–842.
[15] S. T. Schneebeli, M. Kamenetska, Z. Cheng, R. Skouta, R. A. Friesner, L. Venkataraman, R. Breslow, *J. Am. Chem. Soc.* **2011**, *133*, 2136–2139.
[16] F. J. M. Hoeben, P. Jonkheijm, E. W. Meijer, A. P. H. J. Schenning, *Chem. Rev.* **2005**, *105*, 1491–1546.
[17] G. Meyer-Eppler, F. Topić, G. Schnakenburg, K. Rissanen, A. Lützen, *Eur. J. Inorg. Chem.* **2014**, 2495–2501.
[18] S. Cantekin, T. F. A. de Greef, A. R. A. Palmans, *Chem. Soc. Rev.* **2012**, *41*, 6125–6137.
[19] P. J. M. Stals, J. F. Haveman, A. R. A. Palmans, A. P. H. J. Schenning, *J. Chem. Educ.* **2009**, *86*, 230–233.
[20] M. L. Bushey, T.-Q. Nguyen, W. Zhang, D. Horoszewski, C. Nuckolls, *Angew. Chem. Int. Ed.* **2004**, *43*, 5446–5453; *Angew. Chem.* **2004**, *116*, 5562–5570.
[21] a) S. M. Bachrach, *J. Phys. Chem. A* **2011**, *115*, 2396–2401; b) Y. Zhao, D. G. Truhlar, *Theor. Chem. Acc.* **2007**, *120*, 215–241.
[22] Y. Ishida, T. Aida, *J. Am. Chem. Soc.* **2002**, *124*, 14017–14019.
[23] a) J. Guilleme, M. J. Mayoral, J. Calbo, J. Aragó, P. M. Viruela, E. Ortó, T. Torres, D. González-Rodríguez, *Angew. Chem. Int. Ed.* **2015**, *54*, 2543–2547; *Angew. Chem.* **2015**, *127*, 2573–2577; b) J. Kumar, H. Tsumatori, J. Yuasa, T. Kawai, T. Nakashima, *Angew. Chem. Int. Ed.* **2015**, *54*, 5943–5947; *Angew. Chem.* **2015**,

127, 6041 – 6045; c) M. M. Safont-Sempere, P. Osswald, K. Radacki, F. Würthner, *Chem. Eur. J.* **2010**, *16*, 7380 – 7384; d) Z. Xie, V. Stepanenko, K. Radacki, F. Würthner, *Chem. Eur. J.* **2012**, *18*, 7060 – 7070.

[24] H. J. Reich, D. J. Cram, *J. Am. Chem. Soc.* **1969**, *91*, 3527 – 3533.

[25] a) D. Antonov, E. Sergeeva, E. Vorontsov, V. Rozenberg, *Russ. Chem. Bull.* **1997**, *46*, 1897 – 1900; b) V. Rozenberg, N. Dubrovina, E. Sergeeva, D. Antonov, Y. Belokon, *Tetrahedron: Asymmetry* **1998**, *9*, 653 – 656.

[26] a) R. B. Martin, *Chem. Rev.* **1996**, *96*, 3043 – 3064; b) M. M. J. Smulders, M. M. L. Nieuwenhuizen, T. F. A. de Greef, P. van der Schoot, A. P. H. J. Schenning, E. W. Meijer, *Chem. Eur. J.* **2010**, *16*, 362 – 367.

[27] C. Invernizzi, C. Dalvit, H. Stoeckli-Evans, R. Neier, *Eur. J. Org. Chem.* **2015**, 5115 – 5127.

[28] X. Wu, R. Liu, B. Sathyamoorthy, K. Yamato, G. Liang, L. Shen, S. Ma, D. K. Sukumaran, T. Szyperski, W. Fang, L. He, X. Chen, B. Gong, *J. Am. Chem. Soc.* **2015**, *137*, 5879 – 5882.

[29] T. F. A. De Greef, M. M. J. Smulders, M. Wolffs, A. P. H. J. Schenning, R. P. Sijbesma, E. W. Meijer, *Chem. Rev.* **2009**, *109*, 5687 – 5754.

[30] a) M. Kasha, H. R. Rawls, M. A. El-Bayoumi, *Pure Appl. Chem.* **1965**, *11*, 371 – 392; b) M. M. J. Smulders, A. P. H. J. Schenning, E. W. Meijer, *J. Am. Chem. Soc.* **2008**, *130*, 606 – 611.

[31] P. Rademacher in *Modern Cyclophane Chemistry* (Eds.: R. Gleiter, H. Hopf), Wiley-VCH, Weinheim, **2005**, pp. 275 – 310.

[32] D. J. Cram, N. L. Allinger, H. Steinberg, *J. Am. Chem. Soc.* **1954**, *76*, 6132 – 6141.

[33] H. Wolf, M. R. V. Jørgensen, Y.-S. Chen, R. Herbst-Irmer, D. Stalke, *Acta Crystallogr., Sect. B: Struct. Sci., Cryst. Eng. Mater.* **2015**, *B71*, 10 – 19.

[34] CCDC 1497012 [(±)-**1a**] contains the supplementary crystallographic data for this paper. These data can be obtained free of charge from The Cambridge Crystallographic Data Centre.

Received: May 30, 2016
Published online: August 3, 2016

